Research Square

Preprints are preliminary reports that have not undergone peer review.
They should not be considered conclusive, used to inform clinical practice,
or referenced by the media as validated information.

A GA2-oxidase gene introgressed from Cucurbita pepo drives developmental reversal of dominance and semi-dwarfism in Cucurbita moschata

Mingwei Qi
Guangdong Key Laboratory for New Technology Research of Vegetables, Vegetable Research Institute, Guangdong Academy of Agricultural Sciences

Hongbiao Liu
Guangdong Key Laboratory for New Technology Research of Vegetables, Vegetable Research Institute, Guangdong Academy of Agricultural Sciences

Yunying Yao
Guangdong Key Laboratory for New Technology Research of Vegetables, Vegetable Research Institute, Guangdong Academy of Agricultural Sciences

Shudan Xue
Guangdong Key Laboratory for New Technology Research of Vegetables, Vegetable Research Institute, Guangdong Academy of Agricultural Sciences

Yingchao Xu
Guangdong Key Laboratory for New Technology Research of Vegetables, Vegetable Research Institute, Guangdong Academy of Agricultural Sciences

Yujuan Zhong
Guangdong Key Laboratory for New Technology Research of Vegetables, Vegetable Research Institute, Guangdong Academy of Agricultural Sciences

Hexun Huang
Guangdong Key Laboratory for New Technology Research of Vegetables, Vegetable Research Institute, Guangdong Academy of Agricultural Sciences

Wenjun Liu
Guangxi Academy of Agricultural Sciences

Wenlong Luo
luowenlong@gdaas.cn

Guangdong Key Laboratory for New Technology Research of Vegetables, Vegetable Research Institute, Guangdong Academy of Agricultural Sciences

---

Research Article

Keywords: Cucurbita moschata, semi-dwarf, gibberellin 2-oxidase, developmental reversal of dominance, near-isogenic line, introgression

Posted Date: April 14th, 2026

DOI: https://doi.org/10.21203/rs.3.rs-9297032/v1

License: This work is licensed under a Creative Commons Attribution 4.0 International License. Read Full License

Additional Declarations: No competing interests reported.

Abstract

Plant architecture is a key determinant of crop productivity and agronomic efficiency. Here, we report a semi-dwarf *Cucurbita moschata* line, *Sd1*, exhibiting developmental reversal of dominance (DRoD), characterized by early-stage dwarfism followed by partial recovery of stem elongation. Genetic analysis revealed that this phenotype is governed by a dominant dwarf gene, *Sd-1*, and a temporally acting elongation QTL, *Vlp-1*. Fine mapping identified *Sd-1* as a gibberellin 2-oxidase (GA2ox) gene with a protein sequence identical to the *CpDw* allele from *C. pepo*, suggesting interspecific introgression. Promoter variation drives elevated Sd-1 expression, resulting in depletion of bioactive gibberellin (GA_4) and early growth repression. Despite GA deficiency, transcriptomic and hormone profiling revealed early divergence between dwarf and semi-dwarf lines. The semi-dwarf line exhibits increased auxin and salicylic acid levels, which facilitate partial recovery of stem elongation through GA-independent mechanisms. Together, these findings establish a temporal genetic framework for DRoD and highlight the potential of regulatory variation and hormone rebalancing for optimizing plant architecture in cucurbit breeding. These findings reveal a temporally coordinated genetic module linking GA deficiency to hormone-mediated compensatory growth, providing a framework for optimizing plant architecture.

Key message

encodes a GA2ox introgressed from , governs dwarfism in , while QTL mediates transcriptional and metabolic reprogramming to promote GA-independent stem elongation.

Introduction

The genus *Cucurbita* (pumpkins and squash) comprises economically important crops widely cultivated for food, feed, oil production, and ornamental use (Chomicki et al. 2020; Hernandez et al. 2023). Among the cultivated taxa, *C. moschata*, *C. pepo*, and *C. maxima* are the three most extensively grown species worldwide, collectively exhibiting substantial phenotypic diversity and broad environmental adaptability. Notably, *C. moschata* (tropical pumpkin) is distinguished by its strong tolerance to heat, humidity, and diverse pathogens, making it particularly well suited to tropical and subtropical regions.

Plant architecture is a key determinant of crop productivity, planting density, and agronomic efficiency. Dwarf and semi-dwarf phenotypes have played a central role in crop improvement, most notably during the Green Revolution (Evenson and Gollin 2003; Rajendran et al. 2025). Accordingly, dwarfism and compact plant architecture have become major targets in cucurbit breeding (Wang et al. 2022). In recent years, several dwarf genes and quantitative trait loci (QTLs) have been characterized, fine-mapped, or cloned across *Cucurbita* species. In particular, the dominant dwarf loci *CpDw* (widely used in the zucchini group of *C. pepo*) and *CmaDw-1* (*C. maxima*) have been fine-mapped, with candidate genes characterized as encoding gibberellin 2-oxidases (GA2ox; Xiang et al. 2025; Ding et al. 2021). Increased GA2ox activity reduces bioactive GA levels and restricts stem elongation, a conserved mechanism underlying dwarfism in many plants (Buss et al. 2020; He et al. 2024; Liu et al. 2018; Tian et al. 2022). Additional regulators, such as the *Bu* gene encoding a YABBY transcription factor, modulate plant architecture through transcriptional control of stem growth (Li et al. 2024; Wang et al. 2022). While mutations in GA biosynthesis genes (e.g., GA3ox homologs), further highlight the central role of gibberellin metabolism in shaping plant architecture (Wu et al. 2015; Min et al. 2022).

In a previous study, we identified a semi-dwarf *C. moschata* inbred line, *Sd1* (*Semi-dwarf 1*), which is characterized by early-stage dwarfism governed by a dominant dwarf gene *Sd-1* (*Semi-dwarf-1*), followed by partial recovery of stem elongation during mid-to-late development (Luo et al. 2019). This growth pattern represents a typical developmental

reversal of dominance (DRoD), resulting in a compact plant architecture with minimal yield penalty and strong agronomic potential. However, the genetic basis and molecular mechanisms underlying this dynamic phenotype remain unclear.

In the present study, we demonstrate that DRoD in *Sd1* is governed by *Sd-1* in combination with a temporally acting elongation QTL, *Vlp-1* (*Vine length plus 1*). We show that *Sd-1* encodes a GA2ox that is identical to the *CpDw* allele from *C. pepo*, suggesting interspecific introgression. Furthermore, integrative analyses combining transcriptome profiling, hormone quantification and promoter functional assays reveal that elevated expression of *Sd-1* drives gibberellin deficiency, while early transcriptional divergence establishes distinct hormonal trajectories that enable partial recovery of vine elongation. These findings establish a mechanistic framework for developmental reversal of dominance and highlight the potential of temporally regulated genetic modules for precision breeding of plant architecture. Together, our study provides new insights into the temporal genetic regulation of plant architecture in cucurbit crops.

Materials and methods

Plant materials

The semi-dwarf inbred line *Sd1* was developed through 16 generations of crosses between a foreign butternut squash (semi-dwarf and early-flowering) and two local southern Chinese inbred lines (long-vined). Backcross populations (BC_1F_1 to BC_3F_2), derived from a cross between *Sd1* (donor parent) and the long-vine inbred line D205 (recurrent parent), were used for gene mapping. The derived near-isogenic lines (NILs; BC_4F_3) were employed for histological analysis, RNA sequencing, and metabolomic profiling. All plants were grown at the experimental station of the Vegetable Research Institute, Guangdong Academy of Agricultural Sciences, Guangzhou, Guangdong Province, China, under standard agronomic practices.

Phenotyping and morphological characterization

Based on vine elongation dynamics and reproductive transition, plant development in long-vine tropical pumpkin was divided into three stages: (i) early vegetative stage (prior to vine elongation), (ii) elongation stage (from the onset of vine elongation to female flowering), and (iii) reproductive stage (from fruit set to fruit maturity). Under natural conditions in Guangzhou, the early vegetative stage (early stage) typically occurred from 0 to 35 days after transplanting (DAT) in spring or 0 to 20 DAT in autumn, whereas the elongation stage (mid stage) spanned approximately in spring 35 to 60 DAT or 20 to 50 DAT in autumn. Notably, vine elongation usually markedly slows after the transition to reproductive growth, as assimilates are preferentially allocated to fruit development.

Vine length was measured at both early and mid stages. Plant architecture was classified as dwarf (< 1.0 m), semi-dwarf (1.0–2.0 m), or long-vine (> 2.0 m) based on vine length at the time of first female flowering, or at 50 DAT when flowering time varied among genotypes. For inbred line, all measurements were performed on at least three plants per genotype.

Histological investigation

Stem samples were collected from a dwarf NIL (0.1– 0.2 m in plant height at 30 DAT in spring), a semi-dwarf NIL (approximately 0.3– 0.4 m), and the long-vine recurrent parent (0.6– 0.8 m). Internode segments from both basal and

apical regions were harvested for histological analysis. At least three biological replicates were analyzed for each genotype.

Tissues were fixed in FAA solution (70% ethanol, 5% acetic acid, 5% formaldehyde) under vacuum (98 kPa; three cycles of 10 min each), followed by dehydration through a graded ethanol series, clearing in *n*-butanol, and embedding in paraffin. Sections (8 μm thickness) were prepared, mounted on glass slides, and stained with hematoxylin and eosin. Microscopic observations were performed using a stereomicroscope, and cell size was quantified using ImageJ software.

Resequencing and BSA-seq analysis

Genomic DNA was extracted from young leaf tissues using a modified CTAB method (Porebski et al. 1997). Whole-genome resequencing and BSA-seq library construction and sequencing were performed by Biomarker Technologies Corporation (Beijing, China). Approximately 20x depth of clean reads were obtained after removal of adapter sequences and low-quality reads.

For BSA-seq, individuals from the BC_1F_1 population were phenotyped at 35 DAT and classified into three groups (dwarf, semi-dwarf, and long-vine). Equal amounts of DNA from 20–30 individuals per group were pooled to construct three bulks, which were sequenced on Illumina Hiseq4000 platform. Approximately 50x of clean reads for each bulk were aligned to the *C. moschata* reference genome (cv. Rifu v1, http://cucurbitgenomics.org/v2/organism/10) using BWA-MEM with default parameters (Li 2013). Variant calling, including SNPs and InDels, was performed using FreeBayes(Garrison and Marth 2012). High-quality variants were filtered based on read depth and quality threshold by using SAMtools (Li et al. 2009).

BSA analysis was conducted using the R package QTLseqr(Mansfeld and Grumet 2018). The SNP-index for each bulk was calculated, and ΔSNP-index values between contrasting bulks were determined. In addition, the G' (G-prime) statistic was calculated using a tricube smoothing function. Sliding window analysis was performed with a 1 Mb window and a 10 kb step size. Statistical significance thresholds were estimated based on simulations implemented in QTLseqr, and candidate regions were defined as genomic intervals exceeding the confidence limits.

SNP marker development, fine mapping and cloning of Sd-1

SNP markers were developed based on the resequencing data of the donor line Sd1 and the recurrent parent D205. Variants identified within the candidate interval on chromosome 3 were selected for marker development. SNPs with clear polymorphism between the two parents were converted into Kompetitive Allele-Specific PCR (KASP) markers. Primer pairs were designed using Primer3 software and synthesized commercially.

For fine mapping of *Sd-1*, backcross populations (BC_1F_1 to BC_3F_2) were used. At 35 days DAT, individuals exhibiting a clear long-vine phenotype were selected, representing recessive homozygotes lacking the *Sd-1* allele. These individuals were genotyped using KASP markers to identify recombination events within the candidate interval. To identify candidate genes, gene annotation within the fine-mapped interval was retrieved from the *C. moschata* reference genome. Sequence variation analysis based on resequencing data revealed multiple polymorphic genes, among which several showed complete co-segregation with the dwarf phenotype.

The coding sequence and approximately 2 kb upstream promoter region of the candidate gene CmoCh03G013920 were amplified from *Sd1* and D205 using gene-specific primers (Table S1). PCR products were purified and sequenced, and sequence alignment was performed using Multalin(Corpet 1988).

RNA extraction and qRT-PCR analysis

Total RNA was extracted from stem, leaf, root, male flower, and young fruit tissues using the RNAprep Pure Plant Kit (TIANGEN, Beijing, China) following the manufacturer's instructions. RNA integrity was assessed using 1% agarose gel electrophoresis, and concentration and purity were measured with a NanoDrop 2000 spectrophotometer (Thermo Fisher Scientific, USA). First-strand cDNA was synthesized from 1 μg of total RNA using the PrimeScript™ RT reagent Kit with gDNA Eraser (Takara, Dalian, China) according to the manufacturer's protocol.

Quantitative real-time PCR (qRT-PCR) was performed on a CFX96 real-time PCR system (Bio-Rad, USA) using SYBR Premix Ex Taq II (Takara, Dalian, China). Gene-specific primers were designed using Primer3 software and are listed in Table S1. The reaction mixture (20 μL) contained 10 μL of SYBR Premix, 0.4 μL of each primer (10 μM), 2 μL of diluted cDNA, and 7.2 μL of nuclease-free water. The PCR program was: 95°C for 30 s, followed by 40 cycles of 95°C for 5 s and 60°C for 30 s.

Fluorescence data were collected using CFX Manager 3.1 software (Bio-Rad, USA), and relative gene expression levels were calculated using the 2^−ΔΔCt method. Expression was normalized to the internal reference gene *CmEF1α*. Each sample included three biological replicates, each with three technical replicates, and melt curve analysis was performed to verify amplification specificity.

Assay of promoter activity

Promoter activity of *Sd-1* and the long-vine allele (*CmoCh03G013920.1*) was analyzed using *Nicotiana benthamiana* transient expression. Promoter fragments (~ 2 kb upstream of the start codon) were amplified with primers containing *Hind* III and *Bam*H I restriction sites at the 5' ends.

The fragments were cloned into the pGreenII 0800-LUC vector via homologous recombination. Recombinant constructs and empty vector controls were transformed into *Agrobacterium tumefaciens* GV3101 (pSoup). Agrobacterium cultures were grown to mid-log phase, resuspended in infiltration buffer (10 mM MES, 10 mM $MgCl_2$, 300 μM acetosyringone, pH 5.6) to an OD600 of 0.8–1.0, and infiltrated into leaves of 5-week-old *N. benthamiana* plants.

After infiltration, plants were kept in darkness for 12 h, followed by 60 h under a normal photoperiod. At 72 h post-infiltration, leaf discs were collected for dual-luciferase assays. Firefly (LUC) and Renilla (REN) luciferase activities were measured using a dual-luciferase reporter assay kit. Relative transcriptional activity was calculated as the LUC/REN ratio, with 12 biological replicates. For in vivo imaging, leaves were sprayed with 1 mM D-luciferin and imaged using an in vivo imaging system to visualize promoter-driven luminescence.

RNA-seq, metabolomic Analysis, and multi-Omics Integration

Apical stem tissues, including young leaves and vine tips, were collected from *Sd1* NILs at 20 and 40 DAT for transcriptomic and metabolomic profiling. RNA-seq libraries were prepared from 1 μg total RNA per sample, enriched for mRNA, reverse-transcribed into cDNA, and sequenced using 150 bp paired-end reads on the Illumina NovaSeq 6000 platform. Clean reads were aligned to the *C. moschata* reference genome using Hisat2, and differentially expressed genes (DEGs) were identified with $|\log_2 FC| \geq 1$ and adjusted $P < 0.05$ using DEGseq(Wang et al. 2010), followed by GO and KEGG enrichment analyses with clusterProfiler(Yu et al. 2012) and KOBAS 2.0(Xie et al. 2011). For metabolomics, 50 mg of the same tissue was extracted with pre-chilled methanol:acetonitrile:water (2:2:1, v/v/v) and analyzed by UPLC-QTOF-MS on a Waters Acquity HSS T3 column in positive and negative ion modes. Metabolites

were annotated using Progenesis QI with reference to METLIN, public databases, and an in-house library (mass tolerance < 100 ppm for precursors, < 50 ppm for fragments). Transcriptomic and metabolomic data were further integrated to identify correlated pathways and gene–metabolite networks associated with GA-independent vine elongation.

Results

Semi-dwarf resulted from DRoD in C. moschata is driven by a dominant dwarf gene and temporal action of additive elongation QTL

The growth pattern of the semi-dwarf inbred line *Sd1* represents a typical DRoD, characterized by early-stage growth repression followed by partial recovery of elongation. During the early vegetative stage, *Sd1* plants were significantly shorter than the long-vine inbred line D205 (Fig. 1a–b). After approximately 25 DAT in autumn (or 35 DAT in spring), stem elongation partially resumed in *Sd1*; however, both elongation rate and internode length remained lower than those of D205, resulting in a compact semi-dwarf phenotype (Fig. 1c-d). Previously, the early-stage dwarf gene *Sd-1* was mapped to a 0.843 Mb interval in chromosome 3 (Cmo_Chr03: 9.985–10.828 Mb; Luo et al. 2019).

Table 1
Results of BSA-seq on BC_1F_1 pools

Comparison	Method	QTL	Chr	Start	End	Length	nSNPs	Peak position
Dwarf vs long-vine	deltaSNP	1	Cmo_Chr03	10,032,592	10,827,861	795,269	12,166	10,827,861
	Gprime	1	Cmo_Chr03	9,545,112	10,827,861	1,282,749	14,631	10,827,861
Semi-dwarf vs long-vine	deltaSNP	-	-	-	-	-	-	-
	Gprime	1	Cmo_Chr03	9,115,308	10,827,690	1,712,382	9,908	10,827,690
		2	Cmo_Chr17	5,677,962	8,350,394	2,672,432	3,286	6,759,571
Dwarf vs Semi-dwarf	deltaSNP	-	-	-	-	-	-	-
	Gprime	-	-	-	-	-	-	-

To isolate the *Sd-1* allele, we developed backcross populations using *Sd1* as the donor and D205 as the recurrent parent. In the BC_1F_1, some individuals carrying *Sd-1* exhibited relatively faster elongation at 25–30 DAT, suggesting that additional QTLs may modulate stem elongation in the presence of *Sd-1*. We therefore performed bulked-segregant analysis sequencing (BSA-seq) using three phenotypic pools (dwarf, semi-dwarf, and long-vine) sampled at 35 DAT.

BSA between the dwarf and long-vine pools consistently detected a strong signal corresponding to the *Sd-1* locus in both ΔSNP-index and G' analyses (Fig. 1; Table 1). In the semi-dwarf versus long-vine comparison, *Sd-1* was again detected, along with an additional signal on chromosome 17 (Fig. 1f). These results confirm that dwarfism in *Sd1* is primarily controlled by *Sd-1*. Given that late-stage vine length in the F_2 population follows an approximately normal distribution (Luo et al. 2019), the chromosome 17 signal is proposed to represent an additive QTL, designated *Vlp-1* (*Vine length plus 1*), which contributes to mid-to-late-stage stem elongation in the presence of *Sd-1*.

Interestingly, most backcross individuals displaying dwarf phenotypes at the early stage transitioned to semi-dwarf phenotypes at later stages, whereas a subset remained stably dwarf and exhibited impaired floral development and

reduced fruit set under subtropical conditions. These observations support a model in which the temporally distinct actions of *Sd-1* and *Vlp-1* (or additional minor QTLs) underlie DRoD, ultimately generating the semi-dwarf architecture of *Sd1*.

CmoCh03G013920 encodes GA2OX is the candidate gene underlying Sd-1

Through linkage analysis using SNP markers in long-vine plants from backcross populations (BC_1F_1 to BC_3F_2), we fine-mapped *Sd-1* to a 79.6 kb interval (Cmo_Chr03: 10,147,130–10,226,787; Fig. 2). However, mapping region of the *Vlp-1* could not be narrowed down, most likely because of its proximity to the centromeric region and its relatively small, *Sd-1*-dependent phenotypic effect. Through marker-assisted selection combined with phenotypic characterization, we developed two dwarf and seven semi-dwarf NILs carrying *Sd-1*.

To identify candidate genes, we re-sequenced two dwarf NILs, seven semi-dwarf NILs and the recurrent line D205. Genome alignment revealed substantial sequence divergence in the *Sd-1* interval between the donor *Sd1* and both the recurrent parent and the *C. moschata* cv. Rifu reference genome. Within this 79.6 kb region, 16 annotated genes (CmoCh03G013870–CmoCh03G014020) were identified (Table 2), and SNPs in 12 genes (CmoCh03G013880–CmoCh03G013920, CmoCh03G013940–CmoCh03G014010) perfectly co-segregated with the dwarf and long-vine phenotypes. Among them, CmoCh03G013920, encoding a gibberellin 2-oxidase (GA2ox) homologous to *CpDw* in *C. pepo* and *CmaDw-1* in *C. maxima*, is the most promising candidate for *Sd-1*.

Table 2
Gene models in the *Sd-1* mapping region

ID	Position	Annotation
CmoCh03G013870	10,149,548 – 10,152,260	Protein of unknown function
CmoCh03G013880	10,154,669 – 10,158,676	Prefoldin subunit 6
CmoCh03G013890	10,158,868 – 10,165,603	Alpha-1
CmoCh03G013900	10,166,421 – 10,166,779	Protein of unknown function
CmoCh03G013910	10,167,769 – 10,168,056	DUF538 domain-containing protein
CmoCh03G013920	10,170,265 – 10,171,380	Gibberellin 2-beta-dioxygenase
CmoCh03G013930	10,175,781 – 10,182,297	Katanin p60 atpase-containing subunit A-like 2
CmoCh03G013940	10,186,825 – 10,188,523	Glucan endo-1
CmoCh03G013950	10,190,798 – 10,193,035	Protein of unknown function
CmoCh03G013960	10,192,820 – 10,193,080	Outer envelope membrane protein 7
CmoCh03G013970	10,201,389 – 10,203,155	9-cis-epoxycarotenoid dioxygenase
CmoCh03G013980	10,202,480 – 10,203,055	RING-H2 finger protein ATL3
CmoCh03G013990	10,206,960 – 10,210,451	DUF1365 domain-containing protein
CmoCh03G014000	10,214,042 – 10,215,067	Tify domain-containing protein
CmoCh03G014010	10,215,672 – 10,219,434	(S)-2-hydroxy-acid oxidase
CmoCh03G014020	10,221,743 – 10,226,679	KH domain-containing protein At4g18375-like

We next performed transcriptomic and phytohormone profiling on apical internodes of a dwarf NIL, a semi-dwarf NIL, and the recurrent parent at early and mid-growth stages. RNA-seq identified 4,025 differentially expressed genes (DEGs), five of which located within the *Sd-1* interval (Table S2). Importantly, CmoCh03G013920 showed > 10-fold higher expression in both dwarf and semi-dwarf NILs relative to the recurrent parent. Metabolomic analysis revealed bioactive GA_4 was present at 1.45 ng/g in the recurrent parent at 40 DAT but undetectable in the both NILs, directly linking GA2ox overexpression to depletion of active gibberellins.

Taken together, fine-mapping, resequencing, transcriptomic and metabolomic data indicate that CmoCh03G013920 encodes GA2ox and represents the *Sd-1* candidate gene.

The Sd-1 protein identical to C. pepo CpDw and likely originated from interspecies introgression

As the candidate gene of *Sd-1* (CmoCh03G013920) is homologous to *CpDw* (Cp4.1LG10g05910) and *CmaDw-1* (CmaCh03G013990), we performed comparative sequence analyses. Importantly, protein alignment revealed 100% identity between *Sd-1* and *CpDw* (zucchini cultivar X10 and MU-CU-16 reference; Fig. 3a). Analysis of resequencing data further showed that the genomic region surrounding CmoCh03G013920 in *Sd1* differs markedly from that of the recurrent parent D205, but exhibits minimal divergence from the *C. pepo* reference, with only four SNPs located in non-coding regions (Fig. 3b–c). In addition, an approximately 210 kb region flanking *Cp4.1LG10g05910* in Sd1 displays strong synteny with the *C. pepo* genome (Fig. S1).

In contrast, comparison with the long-vine *C. moschata* line identified 25 SNPs within the coding region, including nine non-synonymous substitutions. Collectively, these results provide strong evidence that *Sd-1* was introgressed from *C. pepo* into *C. moschata* through interspecific hybridization.

Elevated Sd-1 (CmoCh03G013920) expression underlies dwarfism

To investigate the molecular basis underlying the dwarf phenotype of *Sd1*, we examined the spatiotemporal expression and transcriptional regulation of *Sd-1* and long-vine allele (*CmoCh03G013920.1*). RT–qPCR analysis revealed that transcript levels were markedly higher in *Sd1* than in D205 across most tissues and stages (Fig. 4). At 15 DAT, expression in *Sd1* was highest in roots and lowest in leaves, with stems showing substantially higher transcript levels than in D205. By 35 DAT, root expression in *Sd1* increased slightly, while stem and leaf expression rose markedly, whereas D205 maintained consistently low expression across all vegetative tissues. In reproductive tissues, transcript abundance in male flowers and young fruits was also elevated in *Sd1* relative to D205. These patterns indicate that the relatively high expression of *Sd-1* in *Sd1* is consistent with its role in GA inactivation and regulation of dwarfism.

Variations in Sd-1 putative promoter region contributes to the elevated expression

To explore potential transcriptional regulatory differences, we sequenced the putative ~ 2 kb promoter region of *Sd-1* (*CmoCh03G013920.1*) and analyzed cis-acting elements using PlantCARE (Supple Fig. 2). Both promoters contained numerous elements associated with light responsiveness, hormone signaling, stress/defense responses, and transcriptional regulation. Notably, the long-vine allele promoter harbored approximately twice as many ethylene-responsive elements and 1.5-fold more MYB-type elements compared with *Sd-1*. In contrast, the *Sd-1* promoter uniquely possessed a low-temperature-responsive element and a light-responsive ACA-motif, whereas the long-vine promoter specifically contained an antioxidant-responsive element, a seed-development regulatory O2-site, and multiple photoperiod/photomorphogenesis-related motifs (AT1-motif, Gap-box, TCCC-motif). These differences in cis-regulatory architecture suggest that *Sd-1* and the long-vine allele (*CmoCh03G013920.1*) may respond differently to environmental signals, hormonal cues, and developmental programs.

To directly test whether promoter sequence differences affect transcriptional activity, we cloned the promoter fragments of both alleles into dual-luciferase reporter vectors. Following transient transformation into *Nicotiana benthamiana* leaves via Agrobacterium-mediated infiltration, in vivo luminescence imaging and luciferase assays consistently showed that the *Sd-1* promoter drives significantly higher transcriptional activity than the long-vine allele promoter, with a relative luciferase activity approximately 1.49-fold higher (Fig. c). This result aligns with the elevated *Sd-1* expression observed in *Sd1* and supports that promoter variation is a key molecular determinant of differential gene expression and the resulting dwarf phenotype.

The declined vine length in NILs mainly arises from reduced cell size in upper internodes

We next performed histological analysis of stem tissues from a dwarf NIL, a semi-dwarf NIL, and the long-vine recurrent parent at mid stage. Both NILs exhibited significantly shorter vine lengths than the recurrent parent, despite having a similar number of nodes (Fig. 6a). In the long-vine parent, internode elongation initiated at approximately the 4th internode and became progressively more pronounced in subsequent internodes, indicating an accelerated growth pattern. In contrast, elongation in the semi-dwarf NIL began later (around the 7th internode) and remained relatively limited, with substantially shorter internodes. In the dwarf NIL, internode elongation was restricted with little to no elongation observed across most nodes.

Cytological analysis revealed that cell size in the upper internodes of both NILs was substantially smaller than that of the recurrent parent (Fig. 6b–d, h–j). In addition, the semi-dwarf NIL exhibited a higher cell number than the dwarf NIL in the same region (115 ± 3.1 vs. 88 ± 3.2 cells per field of view). These results indicate that reduced vine length in the NILs is primarily caused by decreased cell expansion, while increased cell number in the semi-dwarf NIL partially compensates for this reduction, resulting in greater internode elongation compared with the dwarf NIL.

Early transcriptional divergence precedes hormonal and growth differentiation

The semi-dwarf phenotype of Sd1 arises from a temporally coordinated regulatory mechanism. In both dwarf and semi-dwarf NILs, elevated expression of *Sd-1* leads to enhanced gibberellin deactivation and depletion of bioactive GA_4, imposing a strong constraint on stem elongation. Despite this shared GA-deficient background, the two NILs diverge rapidly at the transcriptomic level during early development, prior to detectable differences in vine length.

Table 3
Count of differentially expressed genes between lines

Group	Total	Down	Up
Semidwarf Early vs Dwarf Early	246	94	152
Long-vine Early vs Dwarf Early	1278	773	505
Long-vine Early vs Semidwarf Early	1530	1002	528
Semidwarf Mid vs Dwarf Mid	308	179	129
Long-vine Mid vs Dwarf Mid	1359	944	415
Long-vine Mid vs Semidwarf Mid	1356	939	417
Dwarf Mid vs Dwarf Early	1507	553	954
Semidwarf Mid vs Semidwarf Early	1531	654	877
Long-vine Mid vs Long-vine Early	1062	458	604

At the early stage, 246 DEGs were identified, with a clear upregulation bias in the semi-dwarf NIL (152 up vs 94 down). This pattern was reversed at the mid stage (129 up vs 179 down; Table 3), indicating a dynamic transcriptional shift over development. GO enrichment analysis of early-stage upregulated genes in the semi-dwarf NIL revealed significant enrichment in categories related to peptidase inhibitor activity and amino acid transport (Fig. S3). Enrichment of peptidase inhibitor activity suggests suppression of protein degradation processes, potentially mitigating stress-associated proteolysis. Meanwhile, increased amino acid transport may enhance metabolic capacity and support biosynthetic processes, including auxin production.

At the mid stage, genes downregulated in the semi-dwarf NIL were significantly enriched in GO terms associated with ethylene signaling and hypoxia response such as response to ethylene, ethylene-activated signaling pathway, and cellular response to hypoxia (Fig. S3). Downregulation of these pathways suggests attenuation of ethylene-mediated growth inhibition and alleviation of stress-associated signaling.

Collectively, these results indicate that the semi-dwarf NIL undergoes a temporal shift from early transcriptional activation to mid-stage suppression of stress responses, establishing a growth-permissive state that likely primes subsequent hormonal reprogramming and partial recovery of stem elongation.

Hormone reprogramming and cell expansion underlie GA-independent compensatory growth

The early transcriptional divergence is followed by distinct hormonal trajectories during mid-stage development. The semi-dwarf NIL exhibits increased salicylic acid (SA) accumulation and elevated auxin (IAA) levels (Fig. 7; Table S3). Enhanced SA signaling, potentially mediated by components such as key defense genes (e.g., PR proteins; Table S4), may attenuate excessive stress responses and prevent the establishment of a quasi-constitutive stress response (QCSR). Concurrently, increased auxin accumulation and signaling induce early auxin-responsive genes, particularly members of the SAUR family, which promote cell elongation. This effect is further reinforced by coordinated regulation of cell wall remodeling genes, including upregulation of *XTH6* and repression of *XTH1*, thereby enhancing cell wall extensibility and facilitating internode elongation.

In contrast, the dwarf NIL maintains a stress-dominant hormonal profile, characterized by elevated ABA, JA, and ACC levels, consistent with sustained growth repression. These hormonal differences are reflected at the cellular level,

where the dwarf NIL exhibits reduced cell expansion capacity.

Collectively, these results demonstrate that compensatory growth in *Sd1* occurs independently of gibberellin restoration. Instead, it is achieved through coordinated attenuation of stress signaling and activation of auxin-mediated cell elongation. We propose that developmental reversal of dominance (DRoD) in *Sd1* is driven by a temporally structured regulatory module, in which early transcriptional reprogramming governs downstream hormone balance and cell expansion capacity (Fig. 8). Under persistent GA deficiency, this system enables growth recovery through SA-mediated stress attenuation and auxin-driven cell elongation, providing a conceptual framework for optimizing plant architecture in hormone-limited conditions. This mechanism highlights a GA-independent pathway for growth recovery under sustained hormonal constraint.

Discussion

A temporal genetic framework underlies developmental reversal of dominance

In this study, we uncover semi-dwarf architecture of the *C. moschata* inbred line *Sd1* arises from a temporal decoupling of early-stage dwarfism and subsequent compensatory vine elongation, a process known as developmental reversal of dominance (DRoD), first described in *C. pepo* (Shifriss 1947). We show that this phenotype is governed by the coordinated action of a dominant dwarf gene *Sd-1*, and a temporally acting elongation QTL *Vlp-1*. Specifically, *Sd-1* drives strong repression of stem elongation during early development, whereas *Vlp-1* promotes partial recovery of vine growth at later stages. This temporal partitioning of genetic effects provides a mechanistic explanation for DRoD, in which phenotypic dominance shifts across developmental time. Our findings are consistent with classical observations of DRoD in *Cucurbita* (Shifriss 1947) nd support the view that genetic effects can be developmentally dynamic rather than static (Mackay 2014).

Unlike classical models of dominance that assume static gene effects, our findings highlight that genetic dominance can be developmentally dynamic, governed by stage-specific gene activity and regulatory interactions. This perspective expands the conceptual framework for complex trait regulation, particularly for traits involving growth transitions and developmental plasticity, and underscores the importance of incorporating temporal dynamics into genetic and breeding models.

Introgression and regulatory divergence shape Sd-1 represents a conserved GA2ox module following interspecific introgression

We further characterized that the dominant dwarf gene *Sd-1* encodes a GA2-oxidase that is identical to the *CpDw* allele from *Cucurbita pepo*, providing compelling evidence for interspecific introgression as the origin of this locus in *C. moschata*. Despite identical protein sequences, *Sd-1* exhibits substantially elevated expression across tissues and developmental stages (Fig. 4), which is consistent with in that in *C. pepo* (Ding et al. 2021). We further confirmed this is primarily attributable to cis-regulatory divergence in its promoter region (Fig. 5). This finding underscores the importance of introgression as a mechanism for the transfer of adaptive alleles across species boundaries in *Cucurbita*, as widely documented in crop evolution (Cheng et al. 2019; Hufford et al. 2013; Meng et al. 2025).

Importantly, the *Sd-1* allele expands the functional repertoire of GA2ox genes in cucurbits, demonstrating that quantitative modulation of GA catabolism, rather than complete pathway disruption, can be sufficient to reshape plant architecture. Increased GA2ox activity reduces bioactive GA levels and restricts stem elongation, this dwarfing function of GA2ox homologs is well-conserved across species and have been successfully applied in breeding in

many crops(Buss et al. 2020; Ding et al. 2021; He et al. 2024; Liu et al. 2018; Tian et al. 2022). This highlights the potential of fine-tuning GA catabolism as a versatile and practical strategy for engineering optimal plant architecture in cucurbit crops.

GA-independent compensatory growth in Sd1 is mediated by coordinated transcriptional and hormonal reprogramming

GA deficiency is widely associated with the establishment of a quasi-constitutive stress response (QCSR) state, characterized by upregulation of stress-responsive genes and accumulation of ABA, JA, and ethylene precursors, ultimately leading to sustained growth repression (Achard et al. 2008; Lo et al. 2017). Consistent with this model, the dwarf NIL displayed a stress-dominant transcriptional and hormonal profile, along with reduced cell size in upper internodes, indicating limited cell expansion under persistent QCSR. In contrast, the semi-dwarf NIL partially alleviates this growth restriction through early-stage transcriptional reprogramming, which precedes detectable differences in vine elongation. Notably, this reprogramming is accompanied by attenuation of stress-associated signaling and a shift toward pathways favoring growth.

Metabolomic analyses further reveal that the semi-dwarf NIL adopts a distinct hormonal trajectory under GA deficiency. Enhanced salicylic acid (SA) accumulation at the mid stage, together with activation of *NPR1*-dependent signaling. This may help suppress QCSR by modulating stress-responsive transcription and maintaining redox balance. In particular, SA is known to limit reactive oxygen species (ROS) accumulation and regulate ABA–ROS crosstalk, thereby supporting cellular homeostasis under stress (Aires et al. 2025; Mou et al. 2003; Spoel and Dong 2024). This alleviation of oxidative burden may help maintain cellular homeostasis under GA deficiency.

At the same time, increased auxin (IAA) levels, together with induction of SAUR genes. These changes are accompanied by coordinated regulation of cell wall remodeling genes, including upregulation of *XTH6* and repression of *XTH1*, which likely enhance cell wall extensibility. Auxin has been shown to promote cell elongation through both GA-dependent and GA-independent pathways (Chapman et al. 2012). In particular, auxin-induced SAUR proteins activate plasma membrane H^+-ATPases to drive cell expansion independently of gibberellin signaling(Ren and Gray 2015; Spartz et al. 2014). This mechanism is closely linked to cell wall acidification and remodeling processes that facilitate elongation growth(Du et al. 2020). Together, these changes enhance cell extensibility and support internode compensatory elongation through a GA-independent pathway.

In contrast, the dwarf NIL maintains a QCSR-dominated hormonal state, with elevated ABA, JA, and ACC and limited auxin accumulation, reinforcing growth inhibition. Taken together, these findings demonstrate that coordinated attenuation of stress signaling and activation of auxin-mediated growth pathways underlie compensatory elongation in *Sd1*, providing a mechanistic basis for DRoD under GA deficiency.

Candidate locus Vlp-1 may modulate mid-stage elongation

We demonstrated that the dominant dwarf gene *Sd-1* was introgressed from *Cucurbita pepo* and is identical to the *CpDw* allele. In *C. pepo*, this allele has been reported to confer a stable bush or dwarf growth habit throughout development (Ding et al. 2021). In contrast, in the *C. moschata* background examined here, *Sd-1* induces early-stage dwarfism followed by partial recovery of vine elongation, resulting in a semi-dwarf phenotype. This divergence in phenotypic outcome likely reflects fundamental biological differences between the two species.

C. moschata (tropical pumpkin) is well adapted to tropical and subtropical environments, exhibiting strong tolerance to high temperature and humidity, vigorous vegetative growth, and relatively flexible developmental plasticity (Ferriol and Picó 2008; Paris 2016). In contrast, *C. pepo* (zucchini and summer squash) is typically adapted to temperate climates,

characterized by earlier flowering, a higher proportion of female flowers, and a more determinate or compact growth habit (Paris 2016). These differences suggest that the genetic background of *C. moschata* may buffer or modulate the effects of GA deficiency, allowing recovery of stem elongation at later developmental stages rather than maintaining a constitutive dwarf state as observed in *C. pepo*.

Consistent with this interpretation, most backcross individuals carrying *Sd-1* exhibited a transition from dwarfism at early stages to semi-dwarfism during mid-to-late development. By contrast, a subset of individuals remained severely dwarfed and displayed impaired floral development and reduced fruit set under subtropical field conditions, indicating that sustained GA deficiency imposes strong developmental constraints in this genetic background. These observations further support the idea that additional loci are required to mitigate the growth-inhibitory effects of *Sd-1*.

Our BSA-seq analysis identified a candidate locus on chromosome 17, designated *Vlp-1*, that is associated with mid-stage vine elongation. Although its effect appears modest and mapping resolution is limited due to its proximity to the centromeric region, *Vlp-1* may contribute additively to the partial recovery of internode elongation in the presence of *Sd-1*. At present, however, the evidence remains preliminary. Therefore, *Vlp-1* should be considered a candidate elongation QTL requiring further validation through high-resolution mapping and functional approaches (e.g., CRISPR/Cas9). Importantly, its role is likely supplementary, acting in concert with the broader transcriptional and hormonal reprogramming that underlies developmental reversal of dominance (DRoD) in *Sd1*.

Breeding implications of Sd-1 and future perspectives

In tropical pumpkin production, long-vine cultivars still dominate due to their strong environmental adaptability and yield stability. However, excessive vegetative growth increases labor requirements for pruning and limits planting density, constraining overall productivity. Although a few bush or dwarf genes have been identified (Wang et al. 2022; Wu and Cao 2010; Wu et al. 2015), their adoption remains limited because these genotypes often perform poorly under high temperature, high humidity, and low-light conditions. Such limitations have hindered the practical deployment of compact plant architectures in *C. moschata*.

Our findings suggest that the DRoD-type semi-dwarf architecture represented by *Sd1* provides an effective compromise. By uncoupling early-stage growth restriction with partial recovery of elongation at later stages, the *Sd1* genotype achieves a compact architecture without substantial yield penalty. This growth pattern is consistent with the concept that plant architecture can be optimized through temporal regulation rather than constitutive suppression of growth (Evenson and Gollin 2003). Furthermore, the introgression of *Sd-1* from *C. pepo* (Ding et al., 2021) highlights the value of interspecific gene transfer in expanding the breeding toolkit for cucurbits.

Mechanistically, the *Sd-1–Vlp-1* module highlights a breeding strategy based on temporal regulation of growth. Early GA deficiency restricts elongation, while compensatory hormonal reprogramming and partial mid-stage elongation allow biomass accumulation to continue. This framework demonstrates that plant architecture can be optimized through dynamic rather than static regulation, echoing lessons from semi-dwarf crops during the Green Revolution (Basu and Parida 2023; Robil et al. 2025). More broadly, the DRoD model offers a conceptual approach for designing crop ideotypes that balance growth and stress resilience under hormone-limited conditions, with potential applications beyond cucurbits.

Declarations

Competing Interests

The authors declare no competing interests.

Author Contribution

Wenlong Luo and Wenjun Liu conceived and designed the study, prepared the plant materials and revised the manuscript. Mingwei Qi and Wenlong Luo wrote the manuscript. Hongbiao Liu, Hexun Huang and Wenjun Liu measured the agronomic traits. Mingwei Qi, Yunying Yao, Shudan Xue, Yingchao Xu and Yujuan Zhong performed data analysis and molecular experiments. All authors read and approved the final version of the manuscript.

Acknowledgments

This work was supported by grants from the National Natural Science Foundation of China (32002044) and special Fund for Scientific Innovation Strategy-Construction of 662 Guangdong Academy of Agricultural Sciences (R2017YJ-YB3002).

References

1. Achard P, Renou J, Berthome R, Harberd NP, Genschik P (2008) Plant DELLAs restrain growth and promote survival of adversity by reducing the levels of reactive oxygen species. Curr Biol 18:656–660
2. Aires ES, Ferraz AKL, Ribera LM, Teixeira FP, Carvalho BL, Silva DMR, Freschi L, Rodrigues JD, Ono EO (2025) The application of salicylic acid minimizes the deleterious effects of water deficit in tomato through metabolic and ABA adjustments. Plant Physiol Bioch 229:110417
3. Basu U, Parida SK (2023) Restructuring plant types for developing tailor-made crops. Plant Biotechnol J 21:1106–1122
4. Buss W, Ford BA, Foo E, Schnippenkoetter W, Borrill P, Brooks B, Ashton AR, Chandler PM, Spielmeyer W (2020) Overgrowth mutants determine the causal role of gibberellin GA2oxidaseA13 in *Rht12* dwarfism of wheat. J Exp Bot 71:7171–7178
5. Cheng H, Liu J, Wen J, Nie X, Xu L, Chen N, Li Z, Wang Q, Zheng Z, Li M, Cui L, Liu Z, Bian J, Wang Z, Xu S, Yang Q, Appels R, Han D, Song W, Sun Q, Jiang Y (2019) Frequent intra- and inter-species introgression shapes the landscape of genetic variation in bread wheat. Genome Biol 20:136
6. Chomicki G, Schaefer H, Renner SS (2020) Origin and domestication of Cucurbitaceae crops: insights from phylogenies, genomics and archaeology. New Phytol 226:1240–1255
7. Corpet F (1988) Multiple sequence alignment with hierarchical clustering. Nucleic Acids Res 16:10881–10890
8. Ding W, Wang Y, Qi C, Luo Y, Wang C, Xu W, Qu S (2021) Fine mapping identified the gibberellin 2-oxidase gene CpDw leading to a dwarf phenotype in squash (*Cucurbita pepo* L.). Plant Sci 306:110857
9. Du M, Spalding EP, Gray WM (2020) Rapid Auxin-Mediated Cell Expansion. Annu Rev Plant Biol 71:379–402
10. Evenson RE, Gollin D (2003) Assessing the impact of the green revolution, 1960 to 2000. Science 300:758–762
11. Ferriol M, Picó B (2008) Pumpkin and winter squash. In: Prohens, J., Nuez, F. (eds) Vegetables I. Handbook of Plant Breeding, vol 1. Springer, New York, NY. https://doi.org/10.1007/978-0-387-30443-4_10
12. Garrison E, Marth G (2012) Haplotype-based variant detection from short-read sequencing. arXiv preprint arXiv:1207.3907
13. He Q, Wu H, Zeng L, Yin C, Wang L, Tan Y, Lv W, Liao Z, Zheng X, Zhang S, Han Q, Wang D, Zhang Y, Xiong G, Wang Q (2024) *OsKANADI1* and *OsYABBY5* regulate rice plant height by targeting GIBERELLIN 2-OXIDASE6. Plant Cell

37: koae276

14. Hernandez CO, Labate J, Reitsma K, Fabrizio J, Bao K, Fei Z, Grumet R, Mazourek M (2023) Characterization of the USDA *Cucurbita pepo*, *C. moschata*, and *C. maxima* germplasm collections. Front Plant Sci. https://doi.org/10.3389/fpls.2023.1130814
15. Hufford MB, Lubinksy P, Pyhajarvi T, Devengenzo MT, Ellstrand NC, Ross-Ibarra J (2013) The genomic signature of crop-wild introgression in maize. Plos Genet 9:e1003477
16. Li C, He Z, Li Y, Lan Y, Gong F, Cai P, Yang N, Liu Y, Xia F, Liang G, Liu X (2024) Fine mapping of bush gene and development of molecular marker for bush type in pumpkin (*Cucurbita maxima* Duch.). Agronomy. 14:2967.
17. Li H (2013) Aligning sequence reads, clone sequences and assembly contigs with BWA-MEM. arXiv preprint arXiv:1303.3997
18. Li H, Handsaker B, Wysoker A, Fennell T, Ruan J, Homer N, Marth G, Abecasis G, Durbin R (2009) The Sequence Alignment/Map format and SAMtools. Bioinformatics 25:2078–2079
19. Liu C, Zheng S, Gui J, Fu C, Yu H, Song D, Shen J, Qin P, Liu X, Han B, Yang Y, Li L (2018) *Shortened basal internodes* encodes a gibberellin 2-oxidase and contributes to lodging resistance in rice. Mol Plant 11:288–299
20. Lo S, Ho TD, Liu Y, Jiang M, Hsieh K, Chen K, Yu L, Lee M, Chen C, Huang T, Kojima M, Sakakibara H, Chen L, Yu S (2017) Ectopic expression of specific GA2 oxidase mutants promotes yield and stress tolerance in rice. Plant Biotechnol J 15:850–864
21. Luo W, Wang Q, Li J, Zhong Y, Guo J, Li G, Chen M, Huang H (2019) Characterization of the semi-dwarf germplasm '*CmSd1'*and mapping of the semi-dwarf gene *CmSd-1(t)* in pumpkin (*Cucurbita moschata*). China Cucurbits Veg 32:13–18
22. Mackay TFC (2014) Epistasis and quantitative traits: using model organisms to study gene-gene interactions. Nat Rev Genet 15:22–33
23. Mansfeld BN, Grumet R (2018) QTLseqr: an R package for bulk segregant analysis with next-generation sequencing. Plant Genome-US 11:180006
24. Meng Q, Xie P, Xu Z, Tang J, Hui L, Gu J, Gu X, Jiang S, Rong Y, Zhang J, Udall JA, Grover CE, Zheng K, Chen Q, Kong J, Wang M, Nie X, Lin Z, Jin S, Wendel JF, Zhang X, Yuan D (2025) Pangenome analysis reveals yield- and fiber-related diversity and interspecific gene flow in *Gossypium barbadense* L. Nat Commun 16:4995
25. Min Z, Hu X, Han X, Li Y, Li J, Wang D, Sun L, Sun X (2022) Genetic mapping and identification of the gibberellin 3-oxidase gene *GA3ox* leading to a GA-deficient dwarf phenotype in pumpkin (*Cucurbita moschata* D.). Agronomy 12:1779.
26. Mou Z, Fan W, Dong X (2003) Inducers of plant systemic acquired resistance regulate NPR1 function through redox changes. Cell 113:935–944
27. Paris, H.S. (2016). Genetic Resources of Pumpkins and Squash, *Cucurbita* spp.. In: Grumet, R., Katzir, N., Garcia-Mas, J. (eds) Genetics and Genomics of Cucurbitaceae. Plant Genetics and Genomics: Crops and Models, vol 20. Springer, Cham. https://doi.org/10.1007/7397_2016_3
28. Porebski S, Bailey LG, Baum BR (1997) Modification of a CTAB DNA extraction protocol for plants containing high polysaccharide and polyphenol components. Plant Mol Biol Rep 15:8–15
29. Rajendran S, Chun SM, Kang YM, Hwang GH, Lee DH, Lee SH, Lee B, Kim HC, Bae JH, Kim CM (2025) Small and strong: Dwarf cultivars as a strategic response to shade avoidance syndrome through molecular, hormonal, and breeding innovations. Agron J 117:e70122
30. Ren H, Gray WM (2015) SAUR proteins as effectors of hormonal and environmental signals in plant growth. Mol Plant 8:1153–1164

31. Robil JM, Awale P, McSteen P, Best NB (2025) Gibberellins: extending the Green Revolution. J Exp Bot 76:1837–1853
32. Shifriss O (1947) Developmental reversal of dominance in *Cucurbita pepo*. Proc Amer Soc Hort Sci 50: 330–346
33. Spartz AK, Ren H, Park MY, Grandt KN, Lee SH, Murphy AS, Sussman MR, Overvoorde PJ, Gray WM (2014) SAUR inhibition of PP2C-D phosphatases activates plasma membrane h+-atpases to promote cell expansion in *Arabidopsis*. Plant Cell 26:2129–2142
34. Spoel SH, Dong X (2024) Salicylic acid in plant immunity and beyond. Plant Cell 36:1451–1464
35. Tian X, Xia X, Xu D, Liu Y, Xie L, Hassan MA, Song J, Li F, Wang D, Zhang Y (2022) *Rht24b*, an ancient variation of TaGA2ox-A9, reduces plant height without yield penalty in wheat. New Phytol 233:738–750
36. Wang L, Feng Z, Wang X, Wang X, Zhang X (2010) DEGseq: an R package for identifying differentially expressed genes from RNA-seq data. Bioinformatics 26:136–138
37. Wang S, Wang K, Li Z, Li Y, He J, Li H, Wang B, Xin T, Tian H, Tian J, Zhang G, Li H, Huang S, Yang X (2022) Architecture design of cucurbit crops for enhanced productivity by a natural allele. Nat Plants 8:1394–1407
38. Wang S, Wang K, Li Z, Li Y, He J, Li H, Wang B, Xin T, Tian H, Tian J (2022) Architecture design of cucurbit crops for enhanced productivity by a natural allele. Nat Plants 8:1394–1407
39. Wu T, Cao J (2010) Molecular cloning and expression of a bush related *CmV1* gene in tropical pumpkin. Mol Biol Rep 37:649–652
40. Wu T, Cao J, Qin Z, Du Y (2015) Identification of a novel GA-related bush mutant in pumpkin (*Cucurbita moschata* Duchesne). Pak. J. Bot 47:1359–1366
41. Xiang C, Duan Y, Shu Q, Bo K, Weng Y, Sui X, Wang C (2025). CmaGA2ox2 is associated with dwarf plant architecture controlled by the single dominant *CmaDw-1* locus in Winter squash. Hortic Plant J. https://doi.org/10.1016/j.hpj.2024.12.007
42. Xie C, Mao X, Huang J, Ding Y, Wu J, Dong S, Kong L, Gao G, Li C, Wei L (2011) KOBAS 2.0: a web server for annotation and identification of enriched pathways and diseases. Nucleic Acids Res 39: W316-W322
43. Yu G, Wang L, Han Y, He Q (2012) clusterProfiler: an R package for comparing biological themes among gene clusters. Omics 16:284–287

Figures

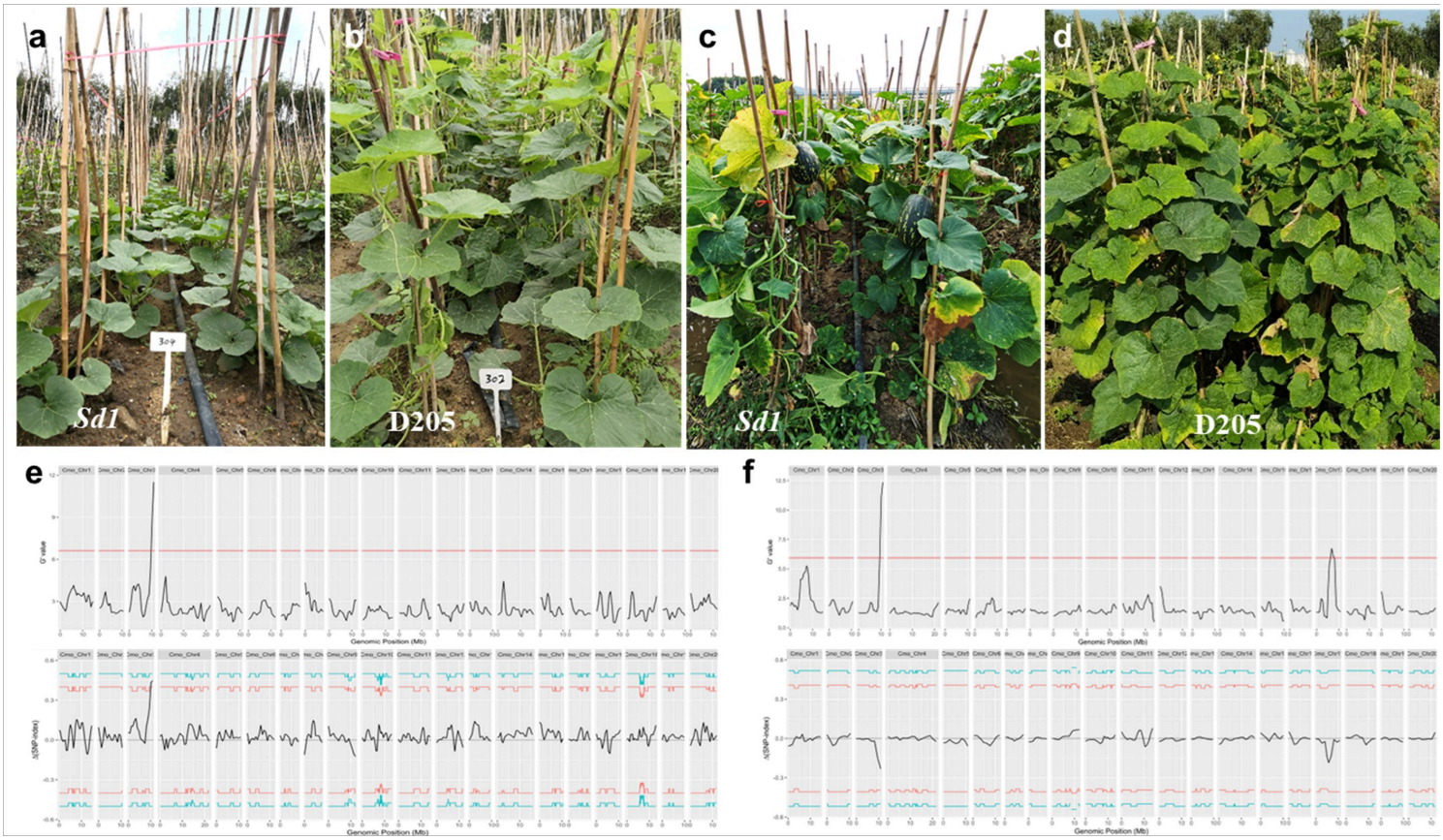


Figure 1

Morphological characterization and genomic mapping of semi-dwarfism in pumpkin. **a-b** Field performance of *Sd1* and long-vine line D205 at 20 days after transplanting (DAT) in autumn. **c-d** Field performance of *Sd1* and D205 at 70 DAT. **e** BSA-seq result of BC_1F_1 dwarf and long-vine pools. **f** BSA-seq result of BC_1F_1 semi-dwarf and long-vine pools.

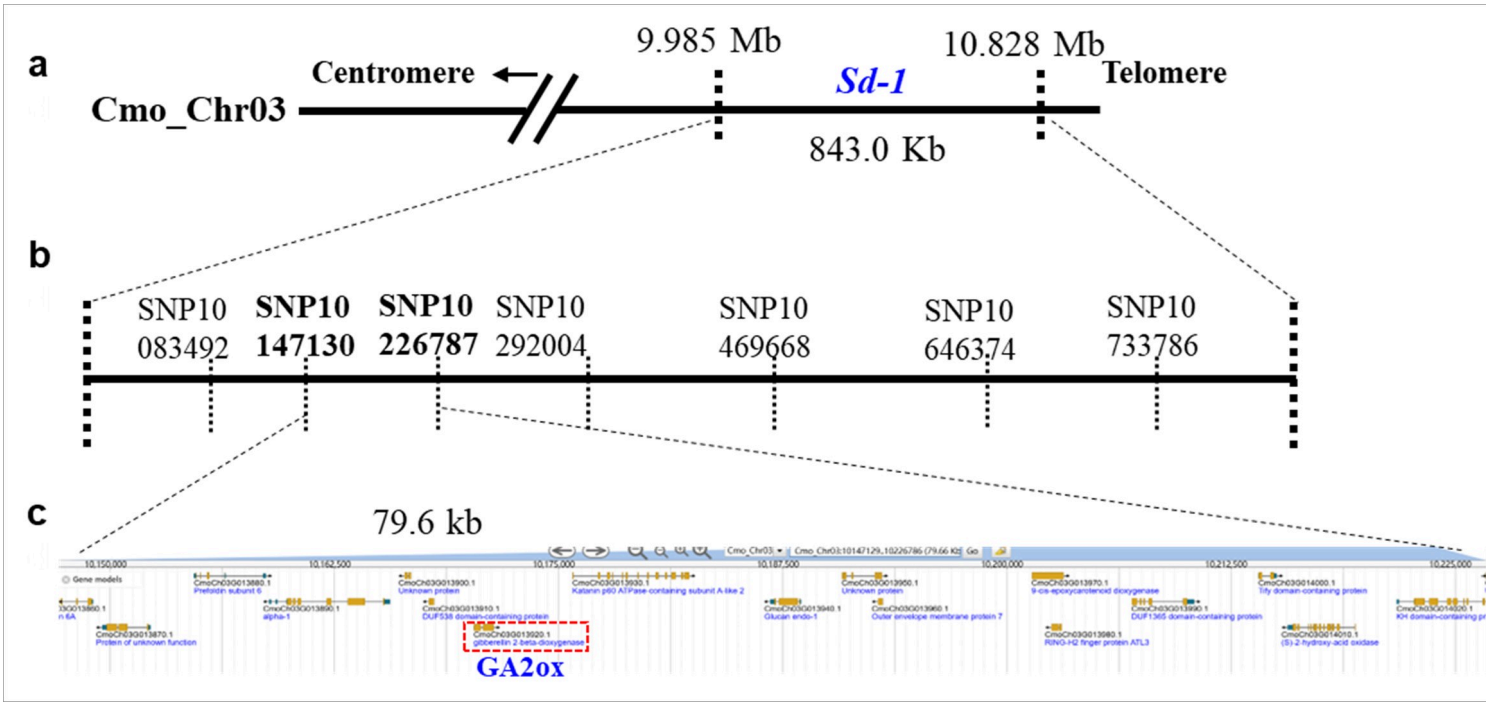


Figure 2

Fine mapping of the *Sd-1*. **a** Primarily mapping region of *Sd-1*. **b** Position of SNPs used for developing KASP marker and linkage analysis. **c** Gene models in the fine mapping region of *Sd-1*. The candidate gene encoding a GA2ox is highlighted in red frame.

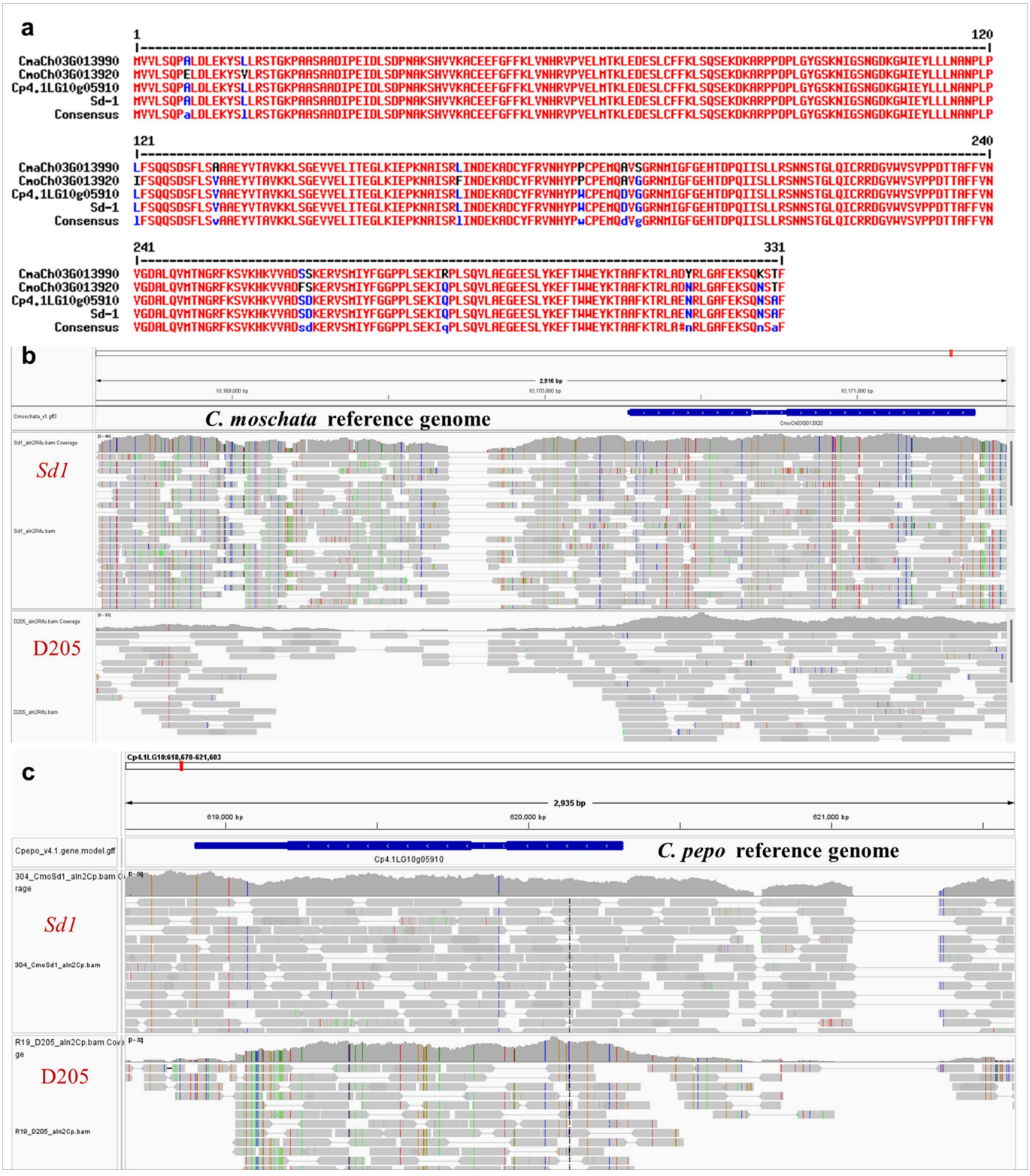


Figure 3

Alignment of protein sequences and genome sequencing reads. **a** Multiple alignment of protein sequences. **b** Alignment of *Sd1* and D205 genomic sequencing reads to *C. moschata* reference genome. **c** Alignment of *Sd1* and

D205 sequencing reads to *C. pepo* reference genome.

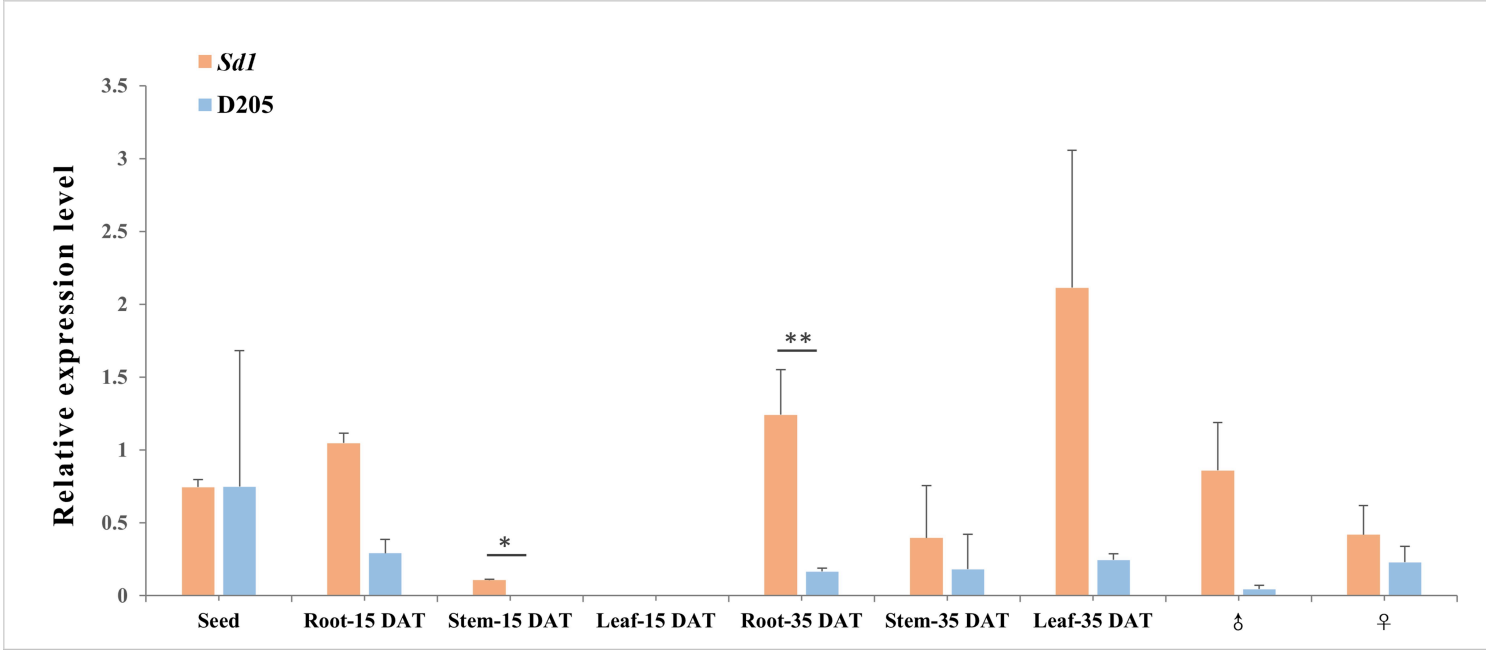


Figure 4

Spatiotemporal expression of *Sd-1* (CmoCh03G013920) in *Sd1* and D205. RT–qPCR analysis shows that *Sd-1* is highly expressed in *Sd1* compared with D205 across most tissues. Data represent mean ± SD from three biological replicates, with statistical significance indicated (*: $p < 0.05$, **: $p < 0.01$).

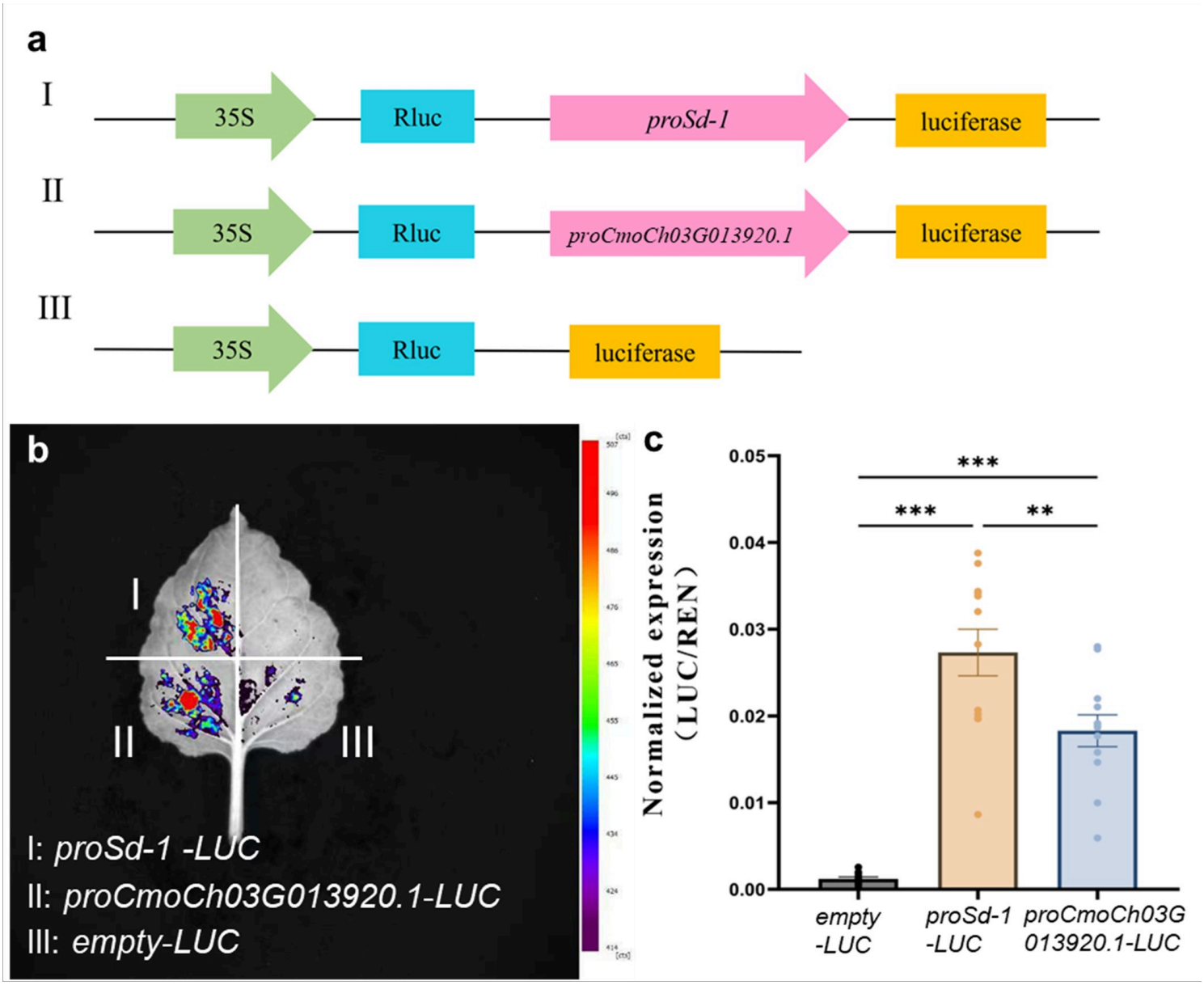


Figure 5

Luciferase reporter assay of *Sd-1* and *CmoCh03G013920.1* promoters. **a** Vector construct; **b** *in vivo* luminescence test images; **c**, normalized relative luciferase activity (LUC/REN ratio). n=8 biological replicates.

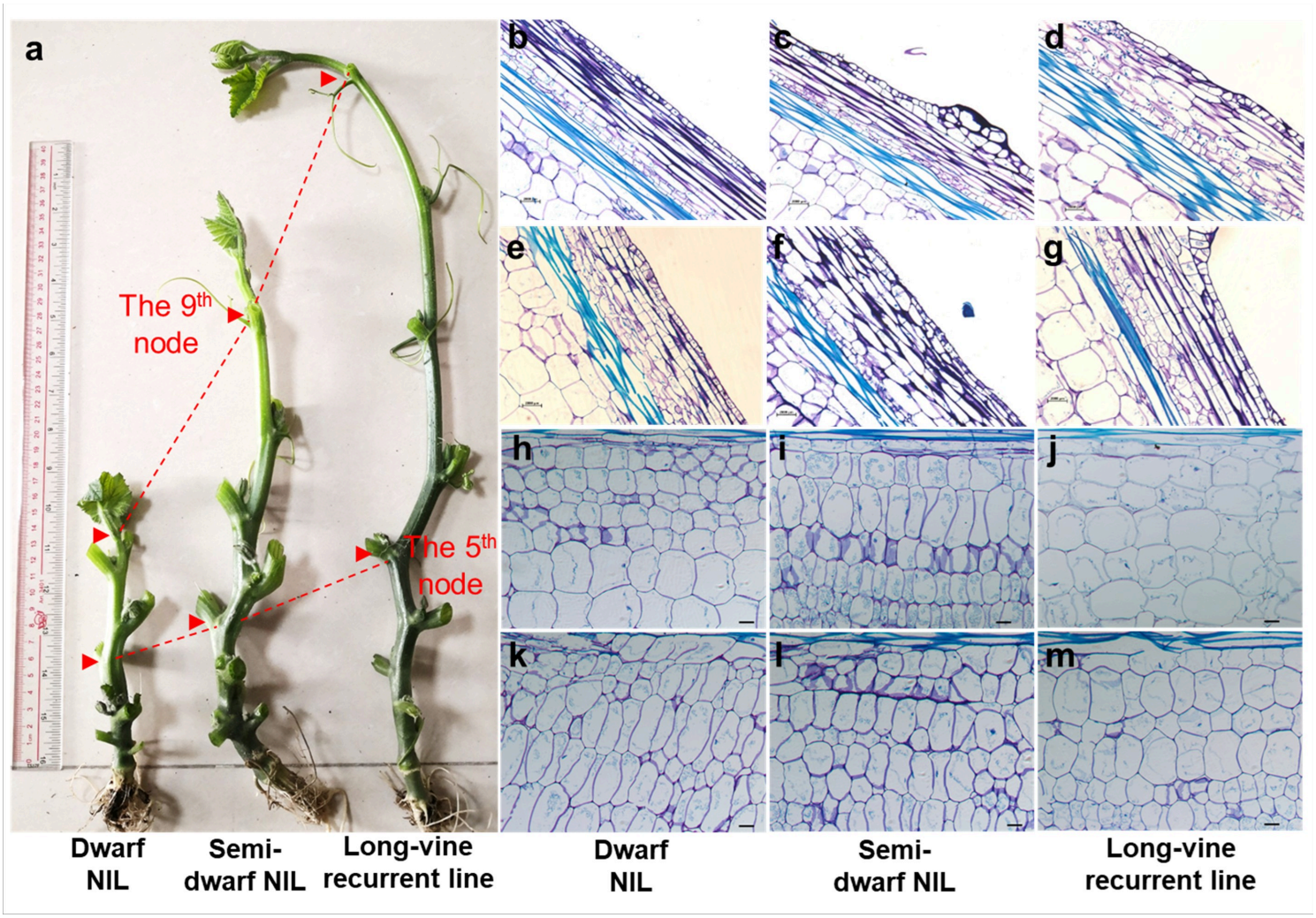


Figure 6

Morphology and cytological examination of backcross progenies. **a** Vine of dwarf NIL, semi-dwarf NIL and recurrent parent line at 35 DAT in spring. **b** to **d** Longitudinal sections of the 7th internode (from bottom) of the three lines. **e** to **g** Longitudinal sections of the 2nd nodes. **h** to **j** Cortex parenchyma cells of the 7th internode. **k** to **m** Cortex parenchyma cells of the 2nd internode. **b** to **g** Bar = 2000 μm. **h** to **m** Bar=500 μm.

	GA4	GA7	GA29	GA24	GA15	GA34	GA51	GA9	ABA	tZ	tZR	IAA	ACC	JA	SA
Dwarf-NIL early	0	0.03	13.17	3.09	4.29	3.95	11.52	0.37	8.90	0.28	1.39	14.17	66.67	7.66	59.59
Semidwarf-NIL early	0	0	11.44	2.35	3.32	2.69	0	0	10.27	0.25	0.78	16.13	51.10	11.16	50.12
Long-vine early	0	0	18.09	3.61	5.52	5.23	9.60	0.40	11.36	0.34	0.60	12.99	119.51	5.84	167.76
Dwarf-NIL mid	0	0.03	29.45	0.76	1.04	2.38	0	0	49.84	0.24	0.36	15.31	88.37	16.86	210.10
Semidwarf-NIL mid	0	0	22.73	0.93	1.43	1.98	0	0	41.72	0.23	0.49	27.83	76.34	9.18	403.53
Long-vine mid	1.45	0	39.76	2.42	5.01	6.85	9.23	0.53	87.28	0.46	1.37	14.20	248.09	12.60	236.99

Figure 7

Determination of hormones in dwarf and semi-dwarf NILs at early and mid-stage. ABA, Abscisic acid; ACC, 1-Aminocyclopropanecarboxylic acid; IAA, Indole-3-acetic acid; JA, Jasmonic acid; SA, Salicylic acid; tZ, trans-Zeatin. The unit of all metabolites were ng/g fresh weight

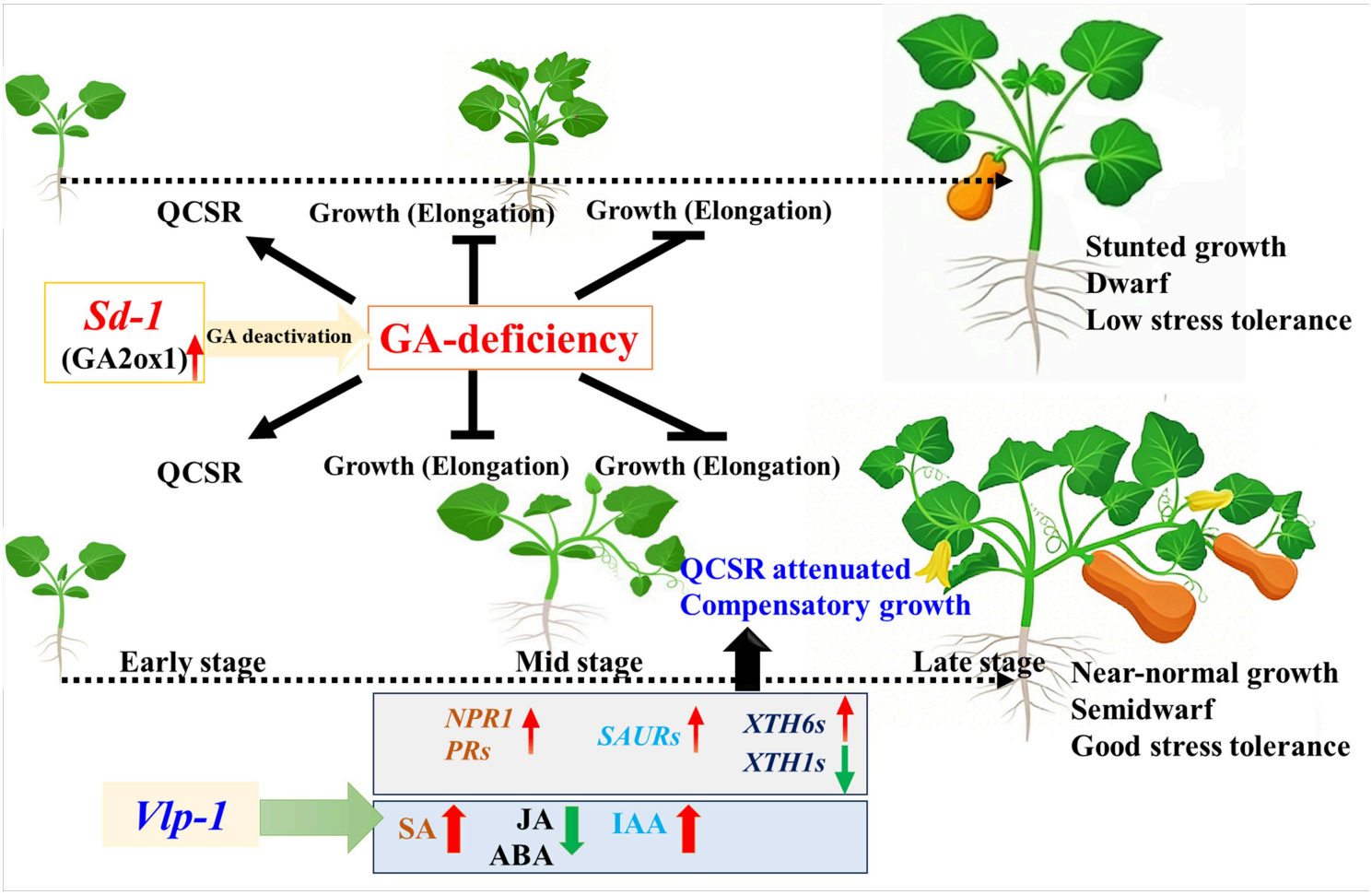


Figure 8

A temporal regulatory model for developmental reversal of dominance (DRoD) in *Sd1*. Under persistent GA deficiency caused by *Sd-1*, early transcriptional reprogramming establishes a growth-permissive state. During mid-stage development, hormonal reprogramming occurs, with increased SA and IAA levels and attenuation of the quasi-constitutive stress response (QCSR). Auxin signaling induces *SAUR*genes and, together with coordinated regulation of *XTH6* and *XTH1*, promotes cell wall extensibility and internode elongation. These processes enable GA-independent compensatory growth, resulting in a near-normal growth and semi-dwarf architecture.

Supplementary Files

This is a list of supplementary files associated with this preprint. Click to download.

- SuppleTablesFigs.docx